Plasma Physics and Controlled Fusion

Transport in stellarators

To cite this article: H Maassberg *et al* 1993 *Plasma Phys. Control. Fusion* **35** B319

Plasma Phys. Control. Fusion 35 (1993) B319–B332. Printed in the UK

TRANSPORT IN STELLARATORS

H. Maaßberg, R. Brakel, R. Burhenn, U. Gasparino, P. Grigull, M. Kick, G. Kühner, H. Ringler, F. Sardei, U. Stroth, and A. Weller

Max-Planck Institut für Plasmaphysik
Association EURATOM-IPP, D-85748 Garching, Germany

Abstract: The local electron and ion heat transport as well as the particle and impurity transport properties in stellarators are reviewed. In this context, neoclassical theory is used as a guideline for the comparison of the experimental results of the quite different confinement concepts. At sufficiently high temperatures depending on the specific magnetic configuration, neoclassical predictions are confirmed by experimental findings. The confinement properties in the LMFP collisionality regime are discussed with respect to the next stellarator generation, for which at higher temperatures the neoclassical transport is expected to become more important.

1. Introduction

The particle and energy transport properties of stellarators and tokamaks in the bulk plasma show some common features, but also significant differences. For the family of quite different stellarator configurations, the main experimental results are briefly reviewed without claim for completeness. The most critical problems of transport in stellarators are discussed with respect to next generation experiments: the Large Helical Device (LHD) [1] being under construction, and W7–X [2, 3], an optimized Helias configuration. These future stellarators, comparable to operating medium size tokamaks, have to demonstrate favourable confinement properties (several keV ion and electron temperatures at densities of up to 10^{20} m^{-3}) essential for demonstrating the reactor potential of the stellarator line.

Present-day stellarators (with major and minor radii up to 2 m and 0.25 m, respectively) have a rather broad spectrum of magnetic configurations [4]. Within the torsatron line, Heliotron-E (Japan) with an aspect ratio of $A \simeq 10$ and $N_p = 19$ field periods, the Advanced Toroidal Facility (ATF, USA) with $A \simeq 8$ and $N_p = 12$, the Compact Helical System (CHS, Japan) with $A \simeq 5$ and $N_p = 8$, and, finally, Uragan–2M (Ukraine, starting operation) with $A \simeq 10$ and $N_p = 4$ have moderate or high shear (with the edge value of the rotational transform $\iota_a \lesssim 1$ except Heliotron-E with $\iota_a \gtrsim 2$). In all these torsatron configurations, the outer part of the plasma confinement region is characterized by rather strong shear and by a magnetic hill. The classical L–2 stellarator (Russia, $A \simeq 8$, $N_p = 14$) with moderate shear, but very large helical ripple is complementary to the nearly shearless W7–A (Germany, $A \simeq 20$, $N_p = 5$, the predecessor of W7–AS) with very small field ripples. The W7–AS stellarator (Germany, $A \simeq 11$, $N_p = 5$) with a full modular coil system is partly optimized with respect to reduced Pfirsch–Schlüter currents (reduction in the Shafranov-shift). W7-AS is also nearly shearless, but has a very complex magnetic field structure (a broad Fourier spectrum of B). Finally, the Heliacs (stellarators with a helical magnetic axis) H-1 (Australia, started operation) and TJ-II (Spain, under construction) with $A \simeq 5$, $N_p = 3$ and $A \simeq 7$, $N_p = 4$, respectively, complete the stellarator family.

In all stellarators, the magnetic field strength, B, shows typically a rather strong modulation along field lines. The radial motion (∇B-drift) of particles trapped in these ripples can

0741-3335/93/000319+14$07.50

affect significantly the confinement properties in the long mean free path (LMFP) regime. In an axisymmetric tokamak, the average radial motion of the "banana" particles cancels, and the neoclassical transport coefficients in the LMFP regime decrease with the collisionality, ν^*, and become negligible. In stellarators, however, the neoclassical transport coefficients increase with $\frac{1}{\nu}$ for decreasing collisionality. A sufficiently large poloidal E × B-rotation can average out the radial ∇B-drift of ripple trapped particles. In the so called $\frac{1}{\nu}$-regime, the neoclassical transport coefficients decrease significantly with the radial electric field, E_r, but this reduction is much stronger for the ions (in tokamaks, there is no E_r dependence in the neoclassical transport coefficients as long as the "banana" orbits exist). The dependence of the neoclassical transport coefficients on E_r can lead to multiple roots of the ambipolarity condition of the particle fluxes [5, 6]. Deep in the LMFP regime, the stellarator-specific "electron root" with large $E_r > 0$ reduces the neoclassical transport coefficients much stronger than the "ion root" with typically $E_r < 0$ (for $T_i \ll T_e$, also $E_r > 0$ is possible). Consequently, the radial electric field plays a very important rôle for the neoclassical transport in stellarators.

With respect to the reactor potential of stellarator configurations, the following aspects are considered to be the most important ones. Firstly, the neoclassical ion heat flux, $Q_i^{\rm neo}$, scales for $E_r = 0$ as $Q_i^{\rm neo} \propto T_i^{9/2}$ in the LMFP regime. As the worst case, this unfavourable T_i-dependence may limit the achievable ion temperatures. Secondly, the temperature gradient drives an outward convective flux which is related to the off-diagonal term in the neoclasscial transport matrix. The balancing diffusive inward term may lead to fairly hollow density profiles in the inner region with negligible particle sources. Finally, accumulation of impurities is neoclassically expected for the "ion root" with $E_r < 0$ which would not allow steady state reactor conditions, the principal advantage of the stellarator line.

2. Global Energy Confinement

As usual, the description of confinement properties has to start with the analysis of global energy confinement. Two types of energy confinement time scalings are available: theory based scalings as, e.g., the Lackner-Gottardi scaling ($\tau_E^{\rm L-G}$) [7] which is based on the neoclassical ion plateau diffusivities or the gyro-reduced Bohm scaling ($\tau_E^{\rm gB}$, e.g., [8]) where a local turbulence model is assumed, and power laws obtained from statistical regression of experimental data as, e.g., the so-called LHD-scaling ($\tau_E^{\rm LHD}$) [9]. The $\tau_E^{\rm L-G}$, $\tau_E^{\rm gB}$ as well as the $\tau_E^{\rm LHD}$ scalings are rather similar, and agree with the experimental τ_E of both stellarators and tokamaks as is shown in Figure 1 for the Lackner-Gottardi scaling. For the different stellarator lines, the global energy confinement is quite similar. The common features of these stellarator-specific τ_E-scalings are the improvement of confinement with volume (roughly with $a^2 R$), with B and with averaged density, $\bar{n}_e$, and the degradation with heating power, P. There is no indication of a dependence on the heating method (e.g., [10]).

Replacing the positive I_p-dependence (plasma current) in the regressional tokamak τ_E-scalings by B and by the edge value of the rotational transform, ι_a, yields much less agreement with the stellarator data. The clear and favourable $\bar{n}_e$-dependence in the stellarator data is not observed in the regressional τ_E-scalings (with strong I_p) of tokamaks, e.g. in the "Goldston L-mode" scaling. No clear indication for an isotope effect is found in stellarators [11].

The nearly shearless stellarators W7–A as well as W7–AS show improving confinement with ι_a as a general trend. Close to low order rational values of ι_a optimum confinement is obtained [43]. In the intermediate ι_a regions, rather strong degradations in τ_E are found. This effect, attributed to the magnetic configuration (see the next Section) is not observed

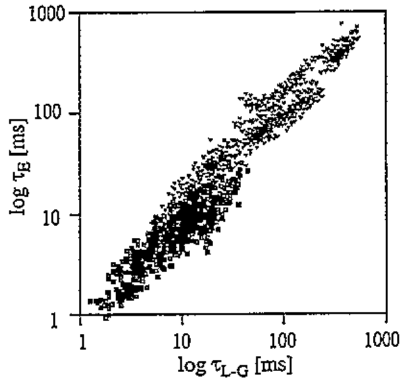

Figure 1: *Experimental energy confinement times of stellarators (□; data from ATF, CHS, Heliotron-E, W7-A and W7-AS) and tokamaks (Y; from ITER L-mode database [12]) versus the Lackner-Gottardi scaling [7]. For this comparison, the plasma current in tokamaks is replaced by B and $\iota(a)$, and $\iota(\frac{2}{3}a)$ is used for the stellarators.*

in stellarators with moderate or high shear. Due to the small plasma size in the present stellarators, the global confinement can be affected by edge effects (e.g. at low order rational values of ι_a).

3. Electron Heat Transport

ECRH discharges at low or moderate densities, for which the collisional power transfer, P_{ei}, allows the separation of the electron and ion power balances, are best candidates for the analysis of the local electron heat transport. The ECRH power deposition is highly localized, and the experimental estimates of the deposition profile (from $T_e(r,t)$ analysis after the ECRH is switched off) are in reasonable agreement with ray-tracing calculations (but, typically, only 50% to 80% of the RF input power is found by this analysis). With the purely diffusive ansatz for the radial electron heat flux density, $q_e = -n_e \chi_e^{\exp} T_e'$, the experimental electron heat diffusivity, $\chi_e^{\exp}$, is derived from the local power balance analysis. These $\chi_e^{\exp}$ values are in reasonable agreement with those obtained from analysis of the heat wave propagation stimulated by ECRH power modulation [14]. In the first part of this section, the so called "anomalous" electron heat transport in stellarators is summarized which is typically found at lower and moderate T_e. The second part deals with the neoclassical effects, found experimentally in case of higher T_e values (within the very LMFP regime).

"Anomalous" electron heat transport:

In stellarators, the T_e profiles reflect the power deposition profiles. "Profile resilience" effects as found e.g. in the D III-D tokamak for off-axis ECRH [15] are not observed. An example for off-axis ECRH at moderate density measured at W7–AS is shown in Figure 2. The hollow T_e profile (due to collisional power loss to the ions, $P_{\rm rad}$ is of minor importance) leads to a $\chi_e^{\exp}$ profile which is compatible, at least within the errors, to that obtained for the equivalent discharge with central ECRH power deposition showing peaked $T_e(r)$ and slightly hollow $n_e(r)$. However, rather small uncertainties in the off-axis power deposition profile result in large errors for the central $\chi_e^{\exp}$. In the example of Fig. 2, $\chi_e^{\exp}$ is much higher than the neoclassical prediction. Contrary to the D III-D results, where a strong inward heat pinch is postulated [15, 16], no indication for a convective term in the electron heat transport is found. This result is supported by analysis of heat waves for off-axis power modulation [17].

In tokamaks, the electron heat transport seems to be linked to the current density profile (e.g., [18]). In stellarators with only rather small toroidal net currents (a few kA), the effect

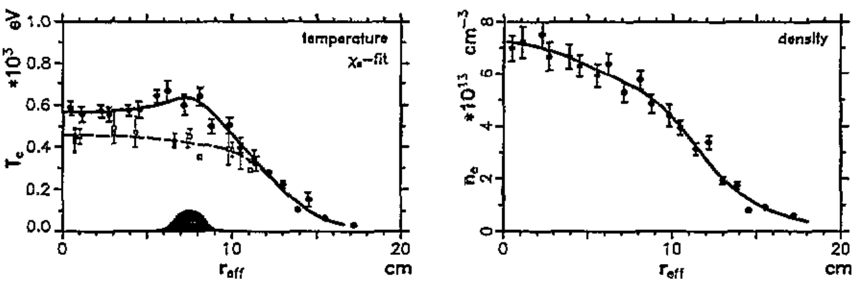

Figure 2: *Electron and ion temperature as well as density profiles of an off-axis ECRH (140 GHz, 2nd harmonic) discharge at W7–AS. The smooth T_e curve is obtained by integration of the electron power balance with a rather flat and purely diffusive $\chi_e^{\rm exp}(r)$. No inward heat pinch is indicated. The indicated ECRH deposition is calculated by ray-tracing consistent with heat wave analysis (ECRH power modulation) as well as with $T_e(r,t)$ analysis after the ECRH is switched off.*

of the internal shear on local transport is also not fully clear. In W7–AS at low order rational values in the $\iota(r)$ profile for low internal shear, confinement degradation is indicated by a local flattening in the T_e profile [19]. At higher internal shear (generated by ECCD, bootstrap and ohmic currents), however, this local confinement degradation disappears. In general, localized mode activity and fluctuations are found at low order rational values in $\iota(r)$ [19, 20].

The effect of external field errors on the magnetic flux surfaces [21] may lead to island formation [22, 24], or, at high shear, to field ergodization. This picture reflects the optimum confinement properties of W7–A as well as of W7–AS close to $\iota_a \simeq \frac{1}{3}$ and $\frac{1}{2}$, where only high order rational values of ι are present. The hypothesis, that the magnetic field in a high shear region can be ergodized (e.g. due to small external error fields), and that parallel electron heat transport is responsible for degraded confinement properties, is not directly confirmed in the experiments. From perturbation field experiments in CHS, Heliotron-E and ATF, no conclusive result related to the ergodization effect is obtained (see, e.g., [23]). Furthermore, in the high shear region in torsatrons close to the plasma edge, where the magnetic hill is present, the electron heat transport may also be attributed to unstable resistive interchange modes [11, 25].

As in tokamaks, the "anomalous" electron heat transport is usually attributed to mode activity and turbulence, but a consistent (at least to some extent) theoretical understanding is missing so far, see, e.g., Ref. 26. Regarding the full 3D and rather complex field topology in stellarators, the theoretical modelling of fluctuations, turbulence and related transport is still at its beginnings. Nevertheless, some general statements seem to be justified. In the torsatrons, an external outward shift of the plasma column or the Shafranov shift of the magnetic axis deepen the magnetic well and increase the radius where the magnetic hill appears. The more favourable MHD properties of these magnetic configurations with respect to global mode activity have been confirmed by Heliotron-E, CHS as well as ATF (e.g., [28]). The better confinement, however, is typically found for the opposite case, i.e. for an inward shift of the magnetic axis. Consequently, the observed low n/m modes do not determine the local electron heat transport. For ATF [11], the dissipative trapped electron mode (DTEM) is discussed to be responsible for the observed $\chi_e^{\rm exp}$. The fraction of trapped particles (controlled externally by the dipole and quadropole moments of the configuration), however, affects only weakly the global confinement properties [8]. Furthermore, no indication for the DTEM is found in CHS [29]. Ballooning modes are not important for stellarator confinement.

The typically "anomalous" χ_e^{exp} obtained from power balance analysis decreases with increasing n_e and B, respectively. A slight improvement with ι for optimum confinement is found in W7–AS [30]. χ_e^{exp} increases with heating power, P. An ECRH power scan (within a factor of 5) shows only a rather small increase in the electron temperature gradient [19]. So far, no regression of $\chi_e^{exp}(r)$ with the power dependence being replaced by the local plasma parameters T_e and T_e' is available. The dependence of $\chi_e^{exp}(r)$ on $T_e(r)$ as well as $T_e'(r)$, which are most relevant to get a feeling for the "anomalous" transport drive, are not yet clear. An other approach is the comparison of dimensionally similar discharges at different B. In stellarators, the χ_e^{exp} profiles are found to be more close to "gyro-Bohm-like" scaling rather than to "Bohm-like" scaling [31]. These findings are different to the JET [32] and TFTR [33] results. The "gyro-Bohm-like" transport scaling may be attributed to radially extended turbulence with correlation lengths of the order of the ion gyro-radius. E.g., the neoclassical transport coefficients, however, are also "gyro-Bohm-like". So far, only preliminary conclusions can be drawn from all these kinds of analysis.

Neoclassical electron heat transport:

For analyzing the neoclassical contribution in the electron heat transport, rather solid theoretical tools (compared to the previous part) are available. In low density ECRH discharges with sufficiently high T_e, the neoclassical heat diffusivity, $\chi_e^{neo} \propto T_e^{7/2}$ in the $\frac{1}{\nu}$-regime, exceeds the "anomalous" one in the inner part of the plasma. By comparing equivalent discharges for W7–A, L–2 and W7–AS, the configurational dependence of $\chi_e^{exp} \approx \chi_e^{neo}$ could be confirmed [34]. The rather poor confinement in L–2 is related to the very large helical ripple, whereas optimum confinement was obtained for W7–A, with the very small field ripples. For electron collisionalities full in the $1/\nu$-regime and with $T_e \gg T_i$, rather strong radial electric fields $E_r > 0$ ("electron root") are predicted for the inner radii. The predicted improved confinement for this "electron root", however, is in contradiction to the experimental power and particle balance. Also at Heliotron-E [35] and CHS [29], neoclassical heat diffusivities are found for equivalent conditions. The E_r values obtained from the measured poloidal plasma rotation are found to be positive as expected, but by a factor of 2 or 3 less than the predicted values of the "electron root" [36]. All these predictions of E_r are mainly based on the ambipolarity condition of the particle fluxes, even if viscosity effects close to the shear layer in the poloidal rotation (transition from "electron" to "ion root", comp. Fig. 5) are taken into account [37]. Possible non-ambipolar contributions (e.g. due to magnetic fluctuations or turbulence) have not been considered.

These results are very significant with respect to the next generation stellarators where at higher T_e, but equivalent collisionalities, sufficiently low electron heat transport has to be demonstrated. As a consequence, attention must be payed to the reduction of the effective helical ripple by optimization of the magnetic configuration. As long as the strong "electron root", which reduces also the neoclassical electron transport coefficients, is not confirmed experimentally, the unfavourable neoclassical electron heat flux ($q_e \propto T_e^{9/2}$ in the $\frac{1}{\nu}$-regime) is expected to exceed significantly the "anomalous" heat transport found in present day tokamak. However, the neoclassical confinement itself can be essentially improved for an optimized magnetic field configuration [3, 38].

4. Ion Heat Transport

At high densities, where the collisional power transfer, $P_{ei} \propto n_e^2(T_e - T_i)/T_e^{3/2}$, causing a strong coupling, the electron and ion heat loss channels cannot be separated based on measured T_e and T_i profiles. Nevertheless, the ion channel seems to play a main role in the power balance. At low densities, P_{ei} becomes small, and only direct ion heating can lead to higher T_i. For NBI sustained discharges at low densities (shortly after the ECRH target phase), rather high ion temperatures (> 1 keV) have been observed [10, 11]. In ATF (at $\bar{n}_e \leq 10^{19}$ m^{-3}), this high T_i-phase immediately after switch-on of the NBI [39] is much shorter than the slowing-down time. These findings may be related to an unstable fast ion distribution leading to preferential ion heating [21] and to rather strong radial electric fields (due to fast ion orbit losses) improving significantly the ion confinement. For this kind of discharges, both the estimation of the degradation in the NBI heating efficiency due to CX losses (which may be essential at low $\bar{n}_e$) and an ion power balance analysis are not available.

In NBI discharges at moderate $\bar{n}_e$ (< 10^{20} m^{-3}), high ion temperatures ($T_e < T_i$ up to 1 keV) were obtained at W7-A [40, 21]. This very good ion energy confinement is attributed to strong $E_r < 0$ generated by fast ion orbit losses of the nearly perpendicular NBI [41, 42]. Although the thermal ions are within the plateau collisionality regime, their neoclassical transport coefficients are significantly reduced by these very large E_r [43, 41]. For this special case, the fast ion orbit losses affected significantly the particle balance (ambipolarity condition). For increased plasma radius as well as for mainly parallel injection, however, fast ion orbit losses are of minor importance. As a consequence, this method to obtain significantly improved thermal ion heat confinement has no prospects.

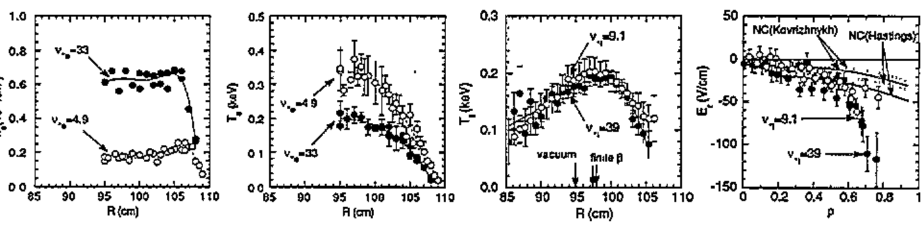

Figure 3: *Density, electron and ion temperature as well as the radial electric field profiles of NBI heated discharges at CHS [44]. The two analytical predictions for E_r: solid lines for high $\bar{n}_e$ (•) and dashed lines for low $\bar{n}_e$ (○).*

For the comparison of the neoclassical ion heat transport with the experimental results, the radial electric field plays an essential role. However, as the E_r profiles are not available in general, neoclassical predictions based on the ambipolarity condition of the particle fluxes are used. Experimental E_r profiles derived from the poloidal plasma rotation measured at CHS [44] are shown in Figure 3. These E_r profiles agree rather well (except for the outer radii) with the neoclassical predictions based on analytical models. For the rather low ion and electron temperatures of this example, the predicted "ion root" is basically confirmed. Nevertheless, the possible effect of non-ambipolar contributions to the particle fluxes can play a role close to the edge (e.g., direct ion loss cone effects).

At W7–AS, the ion power balance is analyzed [45] for both ECRH (with 140 GHz) and NBI discharges (and for combined heating) at moderate densities ($\bar{n}_e$ < 10^{20} m^{-3}). For both types of discharges, the ion heat flux, Q_i^{exp} (estimated from the power balance within 70% of the plasma radius, CX-losses are here negligible), is found to exceed the neoclassical prediction, Q_i^{neo}, with the ambipolar E_r included by a factor of 2 to 3, but to stay well below Q_i^{neo} with $E_r = 0$. As an example, the ion heat flux and the neoclassical prediction are shown in Figure 4 for an ECRH (140 GHz) discharge at optimum confinement. The full

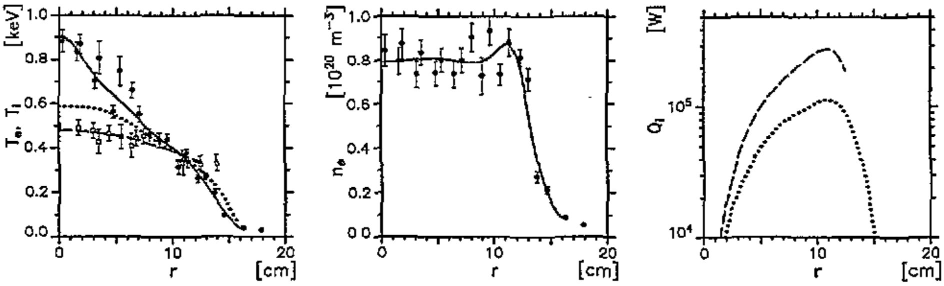

Figure 4: *Profiles of electron and ion temperature (on the left) and density (in the center) of an on-axis ECRH (140 GHz, 2nd harmonic) discharge at W7–AS (after an "H-mode transition"). The additional $T_i(r)$ (dotted line) is the neoclassical prediction (based on DKES code): the self-consistent calculation of both T_i and E_r. In the region where CX-losses are negligible ($r < 12$ cm), Q_i^{exp} from power balance (dashed line, based on the measured T_i) exceeds Q_i^{neo} (dotted line) by a factor of 2 to 3 (on the right).*

T_i-prediction based on neoclassical transport coefficients calculated by the DKES code [46, 47] with the self-consistent E_r (here, only the "ion root" is found) is also given. At lower $\bar{n}_e$ and higher T_i (lower ν_i^*), the effect of E_r on the neoclassical $T_i(r)$ and $Q_i(r)$ is more pronounced. The detailed analysis shows clearly that "convective" terms (non-diagonal elements in the transport matrix being related to both the density gradient and E_r) are important: the comparison of only $\chi_i^{\rm exp}$ (a purely diffusive ansatz for the ion heat transport) with $\chi_i^{\rm neo}$ is not sufficient.

In high power NBI discharges in W7–AS, $\tau_p \gg \tau_E$ is indicated, and $\bar{n}_e$ increases with time. Without efficient density control, the ion collisionality increases within the plateau regime ($Q_i^{\rm neo} \propto n_i T_i^{5/2}$). With efficient density control (low recycling and additonal ECRH, see Sec. 5), stationary conditions are obtained in the transition to the LMFP regime ($\bar{n}_e \simeq 6 \cdot 10^{19}$ m^{-3} and the central $T_i \leq 800$ eV). Here, the ion heat loss is a main part in the total power balance. At lower collisionality, good neoclassical confinement at higher T_i is only predicted for the "electron root" (at rather large $E_r > 0$) with $Q_i^{\rm neo} \propto n_i^2 T_i^{1/2}$ whereas for the "ion root" $Q_i^{\rm neo} \propto T_i^{9/2}$ is expected. Consequently, access to significantly higher ion temperatures should depend on the realization of the "electron root". However, the transition from the "ion" to the "electron root" is predicted only for sufficiently low collisionalities deep in the LMFP regime. $E_r > 0$ was found experimentally in Heliotron-E [35] and CHS [48] only in low density ECRH discharges. As a consequence, the existence of the "electron root" and the associated confinement improvement has still to be experimentally confirmed for higher temperatures and densities.

5. Particle Transport

In general, the density profiles in stellarators and tokamaks are quite different. In stellarators, the density peaking due to an inward convective term is typically not observed. The inner part of the n_e profiles (about 60% to 80% of the plasma radius) is only slightly peaked (typically for NBI) or flat, and for ECRH with central deposition even slightly hollow. An example for an ECRH discharge at W7–AS is shown in Figure 5 (see also [35]). In this discharge, most of the ECRH power was deposited off-axis (at about 8 cm, only 30% highly peaked central deposition). Contrary to the purely off-axis case in Figure 2, the ECRH off-axis

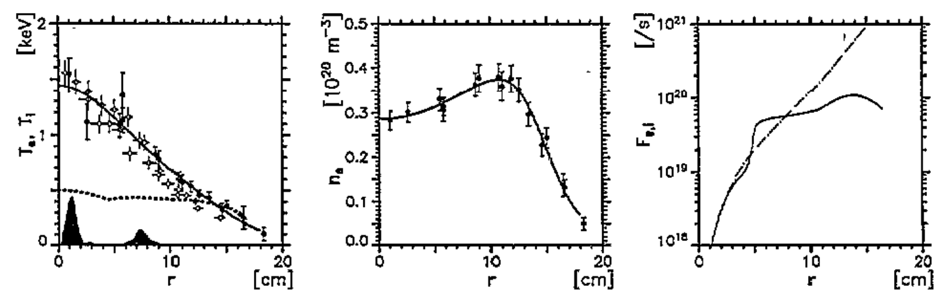

Figure 5: *Profiles of electron and ion (neoclassical prediction) temperature (on the left) as well as density (in the center) of an ECRH (70 GHz, fundamental o-mode) discharge at W7–AS with on- and off-axis power deposition (profile from ray-tracing is indicated). In the inner region, the particle flux,* $\Gamma^{\rm exp}$ *(on the right), estimated by using DEGAS code (dot-dashed line) is in reasonable agreement with the neoclassical (mainly ambipolar) prediction (solid line). At the position of the shear layer in the poloidal plasma rotation* ($r \simeq 5$ *cm), the transition from the inner "electron" to "ion root" at outer radii is related to a small (numerical) viscous flux.*

deposition is not visible in the T_e profile. The 3D distribution of the neutrals is calculated by the DEGAS code [49, 50] (calibrated to H_α-measurements). The averaged particle fluxes, $\Gamma^{\rm exp}$, are estimated and compared with the ambipolar neoclassical predictions, $\Gamma^{\rm neo}$, obtained by using DKES code [46, 47] (s. Fig. 5, on the right). In the region of the hollow density profile, both estimates agree quite well. $\Gamma^{\rm neo}$ is mainly driven by the "convective" term (the non-diagonal term in the transport matrix $\propto T_e'$). Reasonable agreement of $\Gamma^{\rm exp}$ and $\Gamma^{\rm neo}$ is also obtained for low n_e ECRH as well as for high n_e NBI heated discharges in W7–AS [50]. As a consequence, the particle fluxes in the inner part of the plasma are consistent with the neoclassical prediction if the ambipolar radial electric field is taken into account.

At the outer radii, the particle transport analysis based on the neutral gas distribution calculated with DEGAS code leads to "anomalous" particle fluxes (being much larger than $\Gamma^{\rm neo}$). Here the main particle sources (from recycling and from gas puffing) and rather strong density gradients are located. Contrary to tokamaks where an inward particle pinch is required for peaking of the n_e profiles, a purely diffusive ansatz for the particle flux, $\Gamma^{\rm exp} = -D_p n_e'$, seems to be sufficient within the density gradient region [50]. In this region, both the electron heat diffusivity $\chi_e^{\rm exp}$ and D_p show a strong increase towards the plasma edge. Analogous to $\chi_e^{\rm exp}$, D_p decreases with increasing B, n_e and ι_a, and increases with heating power [19]. For W7–AS, Figure 6 shows D_p and $\chi_e^{\rm exp}$ from power balance (both at 80% of the plasma radius) as well as the impurity diffusivities, D_I (from *Al* ablation), versus density. All these transport coefficients scale roughly with n_e^{-1}. The rather large difference in $\chi_e^{\rm exp}$ for the two ι_a values is mainly attributed to the different heating power (P is 3 times larger for $\iota_a = 0.345$ than for $\iota_a = 0.5$), but only a weak effect of P on D_I is indicated. Discharges at equivalent P show clearly a moderate reduction in D_p, D_I and $\chi_e^{\rm exp}$ with ι_a.

With respect to the transport analysis in the stellarator scrape-off layer (SOL), the experimental data base is relatively small compared to tokamaks. Furthermore, due to the very complex stellarator field geometry, theoretical transport modelling in the plasma edge is still in the beginnings. The general findings indicate "anomalous" transport with basic similarities to tokamaks. The observed edge fluctuations (electrostatic turbulence) measured by Langmuir probes are related to particle fluxes, $\Gamma \propto \langle \tilde{n}_e \tilde{\phi} \rangle$, which are roughly consistent (ignoring possible poloidal and toroidal asymmetries in the SOL) with those from the global

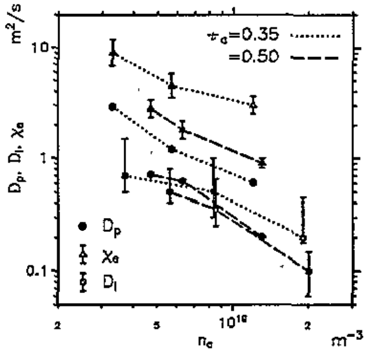

Figure 6: *Particle diffusivity, D_p, and electron heat diffusivity, χ_e^{exp}, versus local density, $n_e(0.8r_a)$, and impurity diffusivity, D_I (obtained by the laser ablation technique), versus central density for ECRH discharges (70 GHz, 2nd harmonic) at W7–AS: $\iota_a = 0.35$ at 550 kW ECRH power (dotted lines) and $\iota_a = 0.50$ at 180 kW (dashed lines).*

particle balance. In W7–AS, SOL Langmuir probe data are analyzed by a 1D radial "flux tube" approach [52] using particle sources (by DEGAS code) and parallel averaging. The D_p obtained within the SOL decrease towards inner radii matching quite well to the inner $D_p(r)$ [53] as obtained by DEGAS code simulations. A scaling of D_p in the SOL inversely to $n_e(r)$ is indicated corresponding to the D_p in the bulk plasma, see Fig. 6. In W7–AS, there is no indication for different transport mechanisms in the density gradient region and in the SOL.

The plasma turbulence at the plasma edge may be related (see, e.g., [54]) to atomic physic processes (radiation, ionization and charge exchange) in combination with non-linear mode coupling [55]. This rather complex drive mechanism is a common feature in stellarators and tokamaks. Inside the plasma, the fluctuation level decreases monotonically. By ECRH power scans, the H_α-signals as well as the global particle confinement clearly indicate a power dependence. With the assumptions that the main turbulence drive is located close to the SOL, and that the turbulence level decays smoothly within the n_e-gradient region, the suggestion of D_p as well as D_I being dependent on P is equivalent to the assumption that the heating power affects the turbulence driving mechanism. It seems to be unlikely that this link is associated with the variation of the edge T_e values [56]. Furthermore, within the n_e' region at ATF, the density fluctuations are attributed to resistive interchange turbulence related to the magnetic hill [57] (opposite to the magnetic well in W7–AS). This mechanism is mainly related to the local plasma parameters.

In high power NBI heated discharges at optimum confinement, n_e increases with time until the discharges are terminated by radiative collapse. A MHD related "density limit" is unknown in stellarators (up to $\bar{n}_e \simeq 3 \cdot 10^{20}$ m^{-3} has been observed in W7–AS). Applying additional ECRH, both density and impurity control can be obtained [10, 51, 19]. So far, a consistent picture for this so called "ECRH pump-out" is missing. In the additional ECRH phase at W7–A [51], the T_e profile broadened whereas the n_e profile was nearly unchanged. Contrary to the remarkable degradation of the global particle confinement, the energy confinement was mainly unaffected. *Al* ablation experiments (see next Sec.) clearly indicate an increase of D_I for the combined phase (a factor of about 3 at Heliotron-E [10]) whereas the inward velocity is only weakly affected. With the assumption of electrostatic turbulence ($\Gamma \propto \langle \tilde{n}\tilde{\phi} \rangle$), these findings suggest an equivalent increase of D_p at least within the n_e' region. In combined ECR and NBI heated discharges in W7–AS, on- or off-axis ECRH deposition can suppress the density increase leading to rather flat n_e and highly or slightly peaked T_e profiles, respectively. After switching-off the ECRH, the T_e profile flattens, and the density starts to increase. These observations show the effect of the T_e profile shaping on the particle transport properties in the inner part (via a non-diagonal term) and, consequently, on the central density evolution.

The "H-mode transition" found in W7–AS [58, 59] shows a steepening of the density gradient only at the outer radii which corresponds to a shrinking of the n_e' region (an increase of T_e' is also observed in this outer region). At the inner radii where $n_e(r)$ is flat, the electron temperature gradient, T_e', is nearly unchanged (but at higher T_e) leading to power balance $\chi_e^{\rm exp}$ which are the same within the error bars. Within the "H-mode" phase (see the profiles of Fig. 4), the reduced gas feed as well as the decreased H_α signals indicate significantly improved particle confinement within the region of steep n_e' just inside the separatrix. First reflectrometry measurements [60] show a significant reduction in the $\tilde{n}_e$ fluctuations being most pronounced at low frequencies (< 10 kHz, corresponding to the long wave lengths) which contribute more efficiently to electrostatic turbulent transport. Assuming $D_p \sim \langle \tilde{n}_e^2 \rangle$, D_p decreases within the n_e' region by a factor of at least 4 which is consistent with the rough estimate from particle balance (reduced gas feed and recycling (H_α) as well as steepening of n_e', no DEGAS simulation being available).

A partly similar transition is also found at W7–AS under limiter conditions at $\iota_a = 0.32$ (and at lower $\bar{n}_e$) [19]: D_p decreases by about 50% in the region of the strong density gradient. The "H-mode-like" NBI heated discharge found at CHS [61] where the rotational transform was increased by an additional ohmic current, is also characterized by a decrease of the H_α signals and by a steepening of the density as well as both temperature gradients close to the edge. All these findings suggest that improved confinement in the steep n_e' region might be due to similar mechanisms in both stellarators and tokamaks.

6. Impurity Transport

The prediction of the impurity fluxes is also closely linked to the radial electric fields. From general arguments, E_r can be identified with a "thermodynamic force" driving "thermodynamic fluxes". For $E_r < 0$, an inward convective term for the ion and, in particlular, for the impurity fluxes ($v_I \propto Z_I E_r / T_i$) is expected. Consequently, neoclassical theory predicts impurity accumulation for strongly negative E_r. Contrary to tokamaks [63], no fully consistent formulation of the neoclassical impurity transport in stellarators is available, so far. From the experimental point of view, impurity transport analysis is based on two approaches: the time analysis of impurity line radiation (with different ionization stages) by laser ablation technique, and the simulation of the accumulation phase.

The analysis of laser ablation experiments is often based on extensive simplifications: e.g., the assumption of $D_I \simeq$ *const.* and $v_I \propto r$ both being the same for all ionization stages. D_I is mainly determined from the increasing line radiation of the highest ionization stages during the inflow phase, whereas the ratio of D_I and v_I by the decay phase. The radiation of low ionization stages, being a convolution of impurity transport, atomic processes and, for the lowest stages, inhomogeneity effects (of the ablated material on flux surfaces), is usually more difficult to simulate. Consequently, these estimates of both D_I and v_I should be interpreted carefully in comparison to the local transport coefficients D_p and $\chi_e^{\rm exp}$. Time-dependent simulations with full radial resolution (e.g, the SITAR code [62]) need more precise experimental data. In general, however, no profile information of the impurity concentrations at the different ionization stages is available. In a predictive version, these codes are used to test theoretical models, e.g., the neoclassical impurity transport. As a consequence, theoretical predictions can only be cross checked with a limited data base.

In low n_e ECRH discharges, no indications for impurity accumulation are found at W7–A, Heliotron-E, ATF and W7–AS. Typically, the average impurity diffusion coefficient, D_I, decreases with increasing $\bar{n}_e$ [10] (see also Fig. 6), and an inward convective term ($v_I < 0$) is not found for these low $\bar{n}_e$. For good confinement properties at high n_e, however, the decay-times, $\tau_{\rm dec}$, of the laser ablated impurity lines become very large, and sometimes, no decay is found within the duration of the discharge. For this type of discharges, also the spectral lines related to wall material (e.g. *Fe*) increase with time indicating "impurity accumulation".

For the NBI heated discharges at W7–A where the optimum ion confinement was attributed to the strongly negative E_r, strong impurity accumulation was found [62]. Fully time-dependent simulations of the impurity transport using a neoclassical, but axisymmetric (tokamak) model (equivalent to [63]) were performed and compared with the experimental findings. Fairly good agreement was obtained. In this axisymmetric model, E_r is implicitly included by "convective" terms related to the background ions, however, these E_r values are less negative than the measured ones (related to the fast ion loss of the nearly perpendicular NBI).

E.g., after the "H-mode transition" impurity accumulation is also indicated at W7–AS. The neoclassical prediction for E_r ("ion root") close to the separatrix yields more negative E_r after the transition. This result is mainly related to the steepening of the density gradient. Consequently, an increased inward velocity in the region of steep n_e' is neoclassically expected. However, both the reduced particle outflux and wall recycling (see Sec. 5) lead to a decreased impurity influx. Strong ELM activity may affect the impurity transport at outer radii (indicated by the outer SX channels). For stationary conditions in the global plasma parameters, the increasing of SX signals and of *Fe* lines indicate accumulation in the bulk part. The radiation level starts to increase already in the phase of good confinement obtained by increasing $\bar{n}_e$. This effect is consistent with the requirement of an inward convective term at higher $\bar{n}_e$ in the analysis of *Si* ablation experiments at Heliotron-E [10] (not so clear in W7–AS, so far). The "H-mode transition" in W7–AS improves mainly the particle confinement just inside the separatrix, and the impurity accumulation becomes more pronounced.

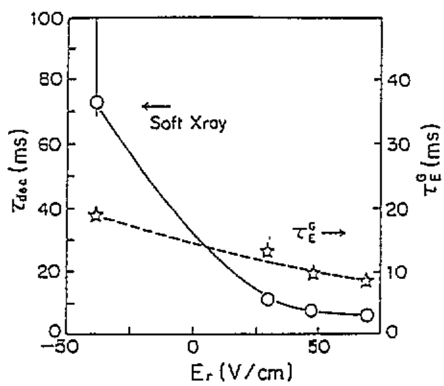

Figure 7: *The decay time, $\tau_{\rm dec}$, of the SX signal after Si laser ablation and the global energy confinement time, τ_E, versus the radial electric field, E_r, measured at about 75% of the plasma radius at Heliotron-E [35]. The E_r was controlled at fixed density ($\bar{n}_e \simeq 10^{19}$ m^{-3}) within an ECRH power scan.*

A very important result is obtained at Heliotron-E [35]. At about 75% of the plasma radius, E_r is deduced from poloidal rotation measurements. At moderate and higher $\bar{n}_e$, the predicted "ion root" with $E_r < 0$ is found. In low density ECRH discharges, positive E_r (possibly the "ion root" for $T_i \ll T_e$) being by a factor of 2 to 3 smaller than the prediction for the "electron root" [36] (comp. also Sec. III) are obtained. Ablation experiments are performed at fixed density ($\bar{n}_e \simeq 10^{19}$ m^{-3}) and with different heating power to control E_r. The decay-time, $\tau_{\rm dec}$, as well as the global energy confinement time are shown in Figure 7 versus E_r. This result demonstrates the strong effect of E_r on the impurity pinch: as $\tau_{\rm dec} \simeq \tau_E$, an outward pinch is indicated for $E_r > 0$. Extrapolating these findings to the high temperature LMFP regime at higher $\bar{n}_e$ being expected for the next generation stellarators, the problem of impurity control is connected to the control of the radial electric field: the realization of the "electron root" (the "ion root" feature with $E_r > 0$ cannot be expected for $T_e \sim T_i$) within the bulk part of the plasma may prevent impurity accumulation.

7. Summary and Conclusions

Transport in stellarators seems to be less sophisticated than in tokamaks. The density and temperature profiles in stellarators reflect mainly the particle and heat sources. It is suggested that ion heat transport as well as particle and impurity transport in the bulk part of the plasma are not so far from the neoclassical predictions, this holds also for the electron heat transport at high electron temperatures. At lower T_e, the experimental electron heat diffusivity is typically "anomalous", however, no indication for a "heat pinch" is found. Similar to tokamaks, this electron heat flux is basically not understood. "Anomalous" particle transport is found in the outer region with steep density gradients where the main particle sources are located. In this region, electrostatic type turbulence seems to be responsible for the particle flux. After "H-mode transitions", the transport coefficients together with the density fluctuations are significantly reduced in the region of steep density gradients.

For the next generation stellarators, much higher electron and ion temperatures are expected. For the "anomalous" electron heat diffusivity, no strong and unfavourable temperature dependence is indicated in the present experiments. The neoclassical transport is expected to become more important which in the stellarator-specific $\frac{1}{\nu}$-regime (LMFP) shows a strong and unfavourable temperature dependence. A classical stellarator configuration with a strong helical ripple will be limited to rather low T_e due to this neoclassical electron heat loss. Consequently, optimization of the magnetic configuration with respect to the reduction of the effective helical ripple is essential [2].

To suppress the unfavourable T_i dependence of the neoclassical ion heat flux, operation under the stellarator-specific "electron root" seems to be desirable. Furthermore, this strongly positive radial electric field could prevent impurity accumulation as it is confirmed experimentally even for rather small $E_r > 0$. However, as the "electron root" solution of the ambipolarity condition is only predicted in the LMFP regime, sufficiently high temperatures are required for the realization of the "electron root". Consequently, this aspect relies on optimized magnetic field configurations with sufficiently low neoclassical losses. So far, the existence of the "electron root" is only predicted theoretically.

The off-diagonal terms in the neoclassical transport connect density and temperature profiles. For the particle transport, no "anomalous" inward convection is experimentally indicated. As the main density gradients (a region of only a few cm, probably not scaling with the plasma radius) are located close to the edge, the temperature gradient driven contribution to the particle flux may result in rather hollow density profiles. As a consequence, also particle sources within the bulk part of the plasma may be necessary in larger stellarators. On the other hand, temperature profile shaping seems to be a possible tool for the control of the density profiles in case of particle sources in the bulk plasma (e.g., for high power NBI heating).

So far, ion temperatures of only up to 1 keV have been obtained in stellarators. It seems to be unlikely, that the rather low T_i values (in comparison to big tokamaks) are only attributed to the smaller plasma radius. Due to the limited temperatures, the full access into the deep LMFP regime with $T_e \simeq T_i$ is hardly possible in the present stellarator experiments. For this regime, however, essential improvements of the neoclassical confinement in the LMFP regime are theoretically predicted for optimized stellarator configurations. Consequently, only the next generation stellarators with significantly increased plasma radius should be able to conclude on the reactor potential of the stellarator line.

Acknowledgements: Helpful discussions with R. Isler, J. Nührenberg and the members of the W7–AS Team are gratefully acknowledged.

References

[1] A. Iiyoshi et al., Fus. Tech. **17**, *169 (1990)*.

[2] G. Grieger et al., Plasma Physics and Controlled Nuclear Fusion Research (Proc. 13th Int. Conf., Washington 1990) Vol. 3, IAEA, Vienna (1991) 525.

[3] G. Grieger et al., Phys. Fluids **B 4**, 2081 (1992).

[4] B.A. Carreras et al., Nucl. Fusion **28**, 1613 (1988).

[5] D.E. Hastings et al., Nucl. Fusion **25**, 445 (1985).

[6] H.E. Mynick, W.N.G. Hitchon, Nucl. Fusion **23**, 1053 (1983).

[7] K. Lackner, N.A.O. Gottardi, Nucl. Fusion **30**, 767 (1990).

[8] M. Murakami et al., *14th International Conference on Plasma Physics and Controlled Nuclear Fusion Research*, Würzburg 1992, paper IAEA-CN-56/C-1-1.

[9] S. Sudo et al., Nucl. Fusion **30**, 1352 (1990).

[10] K. Uo et al., Plasma Physics and Controlled Nuclear Fusion Research (Proc. 11th Int. Conf., Kyoto 1986) Vol. 2, IAEA, Vienna (1987) 355.

[11] M. Murakami et al., Plasma Physics and Controlled Nuclear Fusion Research (Proc. 13th Int. Conf., Washington 1990) Vol. 2, IAEA, Vienna (1991) 455.

[12] P.N. Yushmanov et al., Nucl. Fusion **30**, 1999 (1990).

[13] G. Grieger et al., Plasma Phys. Contr. Fusion **28**, 43 (1986).

[14] L. Giannone et al., Nucl. Fusion **32**, 1985 (1992).

[15] T.C. Luce et al., Phys. Rev. Lett. **68**, 52 (1992).

[16] T.C. Luce et al., *Proc. 8th Joint Workshop on Electron Cyclotron Emission and Electron Cyclotron Resonance Heating*, Gut Ising, Germany 1992, report IPP III/186, Vol. 2, 445 (March 1993).

[17] H.J. Hartfuß et al., *Proc. 8th Joint Workshop on Electron Cyclotron Emission and Electron Cyclotron Resonance Heating*, Gut Ising, Germany 1992, report IPP III/186, Vol. 1, 211 (March 1993).

[18] C.D. Challis et al., Nucl. Fusion **32**, 2217 (1992).

[19] H. Ringler et al., Plasma Phys. Contr. Fusion **32**, 933 (1990).

[20] R. Jaenicke et al., *14th International Conference on Plasma Physics and Controlled Nuclear Fusion Research*, Würzburg 1992, paper IAEA-CN-56/C-2-1.

[21] H. Wobig et al., Plasma Physics and Controlled Nuclear Fusion Research (Proc. 11th Int. Conf., Kyoto 1986) Vol. 2, IAEA, Vienna (1987) 369.

[22] R.J. Colchin et al., Rev. Sci. Instrum. **60**, 2680 (1989).

[23] R.J. Colchin et al., Nucl. Fusion **33**, 323 (1993).

[24] R. Jaenicke et al., Nucl. Fusion **33**, 687 (1993).

[25] T. Obiki et al., *14th International Conference on Plasma Physics and Controlled Nuclear Fusion Research*, Würzburg 1992, paper IAEA-CN-56/C-1-2.

[26] B.A. Carreras, Plasma Phys. Contr. Fusion **34**, 1825 (1992).

[27] T. Obiki et al., Plasma Physics and Controlled Nuclear Fusion Research (Proc. 13th Int. Conf., Washington 1990) Vol. 2, IAEA, Vienna (1991) 425.
[28] M. Wakatani et al., Plasma Physics and Controlled Nuclear Fusion Research (Proc. 13th Int. Conf., Washington 1990) Vol. 2, IAEA, Vienna (1991) 567.
[29] K. Matsuoka et al., Plasma Phys. Contr. Fusion **34**, 1909 (1992).
[30] R. Burhenn et al., 20th EPS Conf. Contr. Fus. Plasma Phys., Lisboa 1993, ECA, Vol. 17C I, 361 (1993).
[31] U. Stroth et al., Phys. Rev. Lett. **70**, 936 (1993).
[32] J.P. Christiansen et al., Plasma Phys. Contr. Fusion **34**, 1881 (1992).
[33] R.J. Hawryluk et al., Plasma Phys. Contr. Fusion **33**, 1509 (1991).
[34] H. Maaßberg et al., Phys. Fluids, in press (1993).
[35] T. Obiki et al., Plasma Physics and Controlled Nuclear Fusion Research (Proc. 12th Int. Conf., Nice 1988) Vol. 2, IAEA, Vienna (1989) 337.
[36] K. Watanabe et al., J. Phys. Soc. Japan **60**, 884 (1991).
[37] H. Maaßberg and K.S. Dyabilin, 20th EPS Conf. Contr. Fus. Plasma Phys., Lisboa 1993, ECA, Vol. 17C I, 409 (1993).
[38] H. Maaßberg, W. Lotz, and J. Nührenberg, Phys. Fluids, in press (1993).
[39] J.F. Lyon, Proc. 8th Int. Stellarator Workshop (IAEA Technical Committee Meeting), Kharkov 1991, p. 7 (1991).
[40] G. Cattanei et al., Plasma Physics and Controlled Nuclear Fusion Research (Proc. 9th Int. Conf., Baltimore 1982) Vol. 2, IAEA, Vienna (1983) 241.
[41] U. Gasparino et al., 19th EPS Conf. Contr. Fus. Plasma Phys., Innsbruck 1992, ECA, Vol. 16C I, 505 (1992).
[42] K. Itoh et al., Nucl. Fusion **32**, 1047 (1992).
[43] G. Grieger et al., Plasma Phys. Contr. Fusion **28**, 43 (1986).
[44] K. Ida et al., Phys. Fluids **B 3**, 515 (1991), and Phys. Fluids **B 4**, 1360 (1992).
[45] M. Kick et al., 20th EPS Conf. Contr. Fus. Plasma Phys., Lisboa 1993, ECA, Vol. 17C I, 357 (1993).
[46] S.P. Hirshman et al., Phys. Fluids **29**, 2951 (1986).
[47] S.P. Hirshman, and W.I. van Rij; Phys. Fluids **B 1**, 563 (1989).
[48] H. Idei et al., 20th EPS Conf. Contr. Fus. Plasma Phys., Lisboa 1993, ECA, Vol. 17C I, 393 (1993).
[49] B.D. Heifetz et al., J. Comput. Phys. **46**, 309 (1982).
[50] F. Sardei et al., 18th EPS Conf. Contr. Fus. Plasma Phys., Berlin 1991, ECA, Vol. 15C II, 193 (1991).
[51] H. Ringler et al., Plasma Physics and Controlled Nuclear Fusion Research (Proc. 11th Int. Conf., Kyoto 1986) Vol. 2, IAEA, Vienna (1987) 603.
[52] F. Sardei et al., J. Nucl. Mater. **196-198**, 443 (1992).
[53] R. Brakel et al., *14th International Conference on Plasma Physics and Controlled Nuclear Fusion Research*, Würzburg 1992, paper IAEA-CN-56/C-2-3.
[54] C. Hidalgo et al., Nucl. Fusion **33**, 146 (1993).
[55] T. Estrada et al., 20th EPS Conf. Contr. Fus. Plasma Phys., Lisboa 1993, ECA, Vol. 17C I, 373 (1993).
[56] C. Hidalgo et al., 20th EPS Conf. Contr. Fus. Plasma Phys., Lisboa 1993, ECA, Vol. 17C II, 733 (1993).
[57] J.H. Harris et al., 19th EPS Conf. Contr. Fus. Plasma Phys., Innsbruck 1992, ECA, Vol. 16C I, 525 (1992).
[58] V. Erckmann et al., *14th International Conference on Plasma Physics and Controlled Nuclear Fusion Research*, Würzburg 1992, paper IAEA-CN-56/H-1-4.
[59] V. Erckmann et al., Phys. Rev. Lett. **70**, 86 (1993).
[60] T. Estrada et al., 20th EPS Conf. Contr. Fus. Plasma Phys., Lisboa 1993, ECA, Vol. 17C I, 369 (1993).
[61] K. Toi et al., 20th EPS Conf. Contr. Fus. Plasma Phys., Lisboa 1993, ECA, Vol. 17C I, 389 (1993).
[62] W7-A Team, NI Group, Nucl. Fusion **25**, 1593 (1985).
[63] S.P. Hirshman, D.J. Sigmar, Nucl. Fusion **21**, 1079 (1981).